Journal of Solid State Chemistry **161,** 166–172 (2001)
doi:10.1006/jssc.2001.9315, available online at http://www.idealibrary.com on IDEAL®

High-Pressure Rare Earth Disilicates $REE_2Si_2O_7$ (REE = Nd, Sm, Eu, Gd): Type K

Michael E. Fleet and Xiaoyang Liu

Department of Earth Sciences, University of Western Ontario, London, Ontario N6A 5B7, Canada

Received April 9, 2001; in revised form July 6, 2001; accepted July 16, 2001

A new structure type (K) is reported for the disilicates of Nd, Sm, Eu, and Gd made at high pressure. Crystals of type K were synthesized at 10 GPa, 1600–1700°C in an MA6/8 superpress and used for single-crystal X-ray structure study by Kappa CCD diffractometry at room temperature. Crystal data are: monoclinic, space group $P2_1/n$, $Z = 4$; $Nd_2Si_2O_7$– $a = 6.6658(2)$, $b = 6.7234(3)$, $c = 12.3975(6)$ Å, $\beta = 102.147(3)°$, $V = 543.2$ Å^3, $R = 0.029$, and $D_x = 5.584$ g/cm^3; $Sm_2Si_2O_7$– $a = 6.6039(3)$, $b = 6.6849(3)$, $c = 12.3069(5)$ Å, $\beta = 102.489(3)°$, $V = 530.4$ Å^3, $R = 0.038$, and $D_x = 5.871$ g/cm^3; $Eu_2Si_2O_7$– $a = 6.5777(3)$, $b = 6.6652(4)$, $c = 12.2668(8)$ Å, $\beta = 102.671(4)°$, $V = 524.7$ Å^3, $R = 0.030$, and $D_x = 5.976$ g/cm^3; $Gd_2Si_2O_7$– $a = 6.5558(4)$, $b = 6.6469(4)$, $c = 12.2394(6)$ Å, $\beta = 102.844(3)°$, $V = 520.0$ Å^3, $R = 0.026$, and $D_x = 6.166$ g/cm^3. The type K structure is built from a diorthosilicate group [Si_2O_7] interconnected by REE^{3+} cations in eightfold coordination with oxygen. The bridging oxygen (Si–O–Si) bond angle of the diorthosilicate group of rare earth disilicates stable at 1 bar (types A to G) is related to spatial accommodation of the REE^{3+} cation and ranges from 130 to 135° in the light rare earth disilicates (types A, F, G) to 180° in $Lu_2Si_2O_7$ (type C). Volume reduction in the high-pressure type K structure is achieved largely by closure of the Si–O–Si bond angle to 122.7–124.4°, through rigid body rotation of the two SiO_4 tetrahedra. This also permits a marginal increase in the average coordination of the REE^{3+} cation. © 2001 Academic Press

Key Words: **rare earth disilicates; $Nd_2Si_2O_7$; $Sm_2Si_2O_7$; $Eu_2Si_2O_7$; $Gd_2Si_2O_7$; high-pressure silicates.**

INTRODUCTION

The structures of the rare earth element (REE) disilicates vary with both position in the lanthanide series (or size of the REE^{3+} cation) and temperature, at low pressure (1 bar to 0.2 GPa). Seven distinct structure types (A to G) have been identified (1) and were reported in (2–15). In six of these structure types (A, C, D, E, F, and G) the SiO_4 tetrahedra are associated into diorthosilicate [Si_2O_7] groups, and the structures essentially represent different ways of packing diorthosilicate groups and REE^{3+} cations present in the ratio 1 : 2. The seventh structure type (B), which is adopted by the disilicates of Eu, Gd, Tb, Dy, Ho, and Er at the lowest temperatures investigated (i.e., below 1000–1450°C), is very unusual in having the SiO_4 tetrahedra in a one-to-one combination of a single (isolated) tetrahedron and a linear triple tetrahedral group [Si_3O_{10}]. The type B structure was reported originally for $Ho_2Si_2O_7$ (7) and was recently confirmed for $Dy_2Si_2O_7$ (15). The monotonic decrease in size of the REE^{3+} cation through the lanthanide series has a considerable influence on structure type of rare earth compounds. Mean REE^{3+}-O bond distances in the REE disilicates were compared with the effective bond distances for six-, seven-, eight-, and ninefold coordination of REE^{3+} with oxygen in Fleet and Liu (15). The data for the REE disilicate structure types exhibited discontinuities representing the limits of accommodation of the REE^{3+} cation by individual structure types. There was a tendency for a given structure type to define a mean REE^{3+}-O bond distance that tended to be greater than the sum of effective cation–anion radii (16) at the lower end of the cation size range of a given structure type and correspondingly smaller at the higher end.

The present study is part of a systematic investigation of the polymorphism of the rare earth disilicates at moderate and high pressure. We reasoned that with an increase in pressure of synthesis, the fields of structure types in Fig. 1 of Felsche (1) might shift progressively toward the Lu end of the lanthanide series, reflecting progressive increase in coordination of the REE^{3+} cation. Alternatively, volume change might be dominated by rotation of the "rigid" SiO_4 tetrahedra in diorthosilicate units (cf., 17–20). We report that disilicates of Nd, Sm, Eu, and Gd synthesized at 10 GPa have a new structure type (K) and that compression is accomplished mainly by decrease in the bridging oxygen (Si–O–Si) bond angle, which is commonly known as the dihedral angle of the diorthosilicate group.

EXPERIMENTAL PROCEDURES

The high-pressure rare earth disilicates were synthesized using the MA6/8 superpress at the University of Alberta,

0022-4596/01 $35.00

TABLE 1
Experimental Details

	$Nd_2Si_2O_7$	$Sm_2Si_2O_7$	$Eu_2Si_2O_7$	$Gd_2Si_2O_7$
Experiment (#)	3138	3168	3169	3137
Pressure (GPa)	10	10	10	10
Temperature (°C)	1600	1700	1700	1600
Time (h)	24	12	12	24
Crystal size ($mm^3 \times 10^4$)	0.81	4.7	1.5	0.65
Crystal shape	prism	tablet	equant	tablet
a (Å)	6.6658(2)	6.6039(3)	6.5777(3)	6.5558(4)
b (Å)	6.7234(3)	6.6849(3)	6.6652(4)	6.6469(3)
c (Å)	12.3975(6)	12.3069(5)	12.2668(8)	12.2394(6)
β (°)	102.147(3)	102.489(3)	102.671(4)	102.844(3)
Space group	$P2_1/n$	$P2_1/n$	$P2_1/n$	$P2_1/n$
Formula weight	456.7	468.9	472.1	482.7
D_x (g/cm^3)	5.584	5.871	5.976	6.166
Reflections—unique	2385	1560	1536	1526
Reflections—number, with ($I < 3\sigma_{(I)}$)	1153	383	557	663
Refined parameters	101	101	101	101
μ (cm^{-1})	193.3[a]	223.6[b]	241.3[b]	257.3[a]
R	0.029	0.038	0.030	0.026
R_w	0.026	0.046	0.026	0.024
s	0.914	1.115	1.074	0.851
g ($\times 10^4$)	0.39(1)	0.50(2)	0.143(9)	0.21(1)
$\Delta\rho$ (eÅ^{-3}) (+)	1.86	3.00	2.19	1.44
(−)	1.86	3.92	1.86	1.74

[a] Gaussian absorption correction.
[b] Empirical absorption correction.

Edmonton (Table 1). All experiments were run in Pt capsules embedded in an octahedral medium made of MgO-5%Cr_2O_3, with an edge length of 14 mm, using $LaCrO_3$ furnaces (21), and monitored with $W_{95}Re_5$–$W_{74}Re_{26}$ thermocouples. All furnace parts were previously fired at 1000°C in air. The capsules were not dried before welding shut and the assemblies with capsules inserted were stored at 110°C prior to the experiments. Starting materials were high purity REE^{3+} oxides and amorphous silica (Aldrich Chemical Co.), which were mixed in stoichiometric proportions and reacted at 950°C for 2 h in Pt crucibles. The experiments were temperature quenched by switching off the power to the furnace at the experimental pressure. Quench rates at high temperature were estimated to be about 1000°C/s. The product of all opened capsules was single-phase rare earth disilicate, which was present as a few 10–100 μm diameter fragments of single crystals and finer-grained crystalline material. The proportion of large crystal fragments to fine-grained matrices varied from one experiment to another.

The crystal fragments of rare earth disilicates were characterized using single-grain Gandolfi powder X-ray diffraction (P-XRD), and the fine-grained matrices were characterized by using petrographic optical microscopy. Crystals of $Nd_2Si_2O_7$ and $Gd_2Si_2O_7$ were further investigated by electron probe microanalysis (EPMA) using a JEOL 8600 Superprobe. Operating conditions included

TABLE 2
Positional and Isotropic Thermal Parameters (Å^2)
($B_{eq} = 4/3 \sum_i \sum_j \beta_{ij} a_i.a_j$)

		$Nd_2Si_2O_7$	$Sm_2Si_2O_7$	$Eu_2Si_2O_7$	$Gd_2Si_2O_7$
X[a](1)	x	0.17108(4)	0.16850(6)	0.16795(5)	0.16729(5)
	y	0.89475(4)	0.89384(6)	0.89377(5)	0.89370(5)
	z	0.63907(2)	0.63839(3)	0.63822(3)	0.63791(3)
	B_{eq}	0.671(6)	0.56(1)	0.723(9)	0.694(8)
X(2)	x	0.20339(4)	0.19934(6)	0.19756(5)	0.19628(6)
	y	0.68497(4)	0.68248(6)	0.68233(5)	0.68188(5)
	z	0.34238(2)	0.34336(3)	0.34375(3)	0.34417(3)
	B_{eq}	0.718(6)	0.61(1)	0.81(1)	0.761(9)
Si(1)	x	0.6901(2)	0.6888(3)	0.6881(3)	0.6882(3)
	y	0.8258(2)	0.8258(3)	0.8256(3)	0.8254(3)
	z	0.5854(1)	0.5852(2)	0.5848(2)	0.5848(2)
	B_{eq}	0.47(2)	0.41(4)	0.55(3)	0.52(3)
Si(2)	x	0.6877(2)	0.6846(4)	0.6827(3)	0.6811(3)
	y	0.5745(2)	0.5746(3)	0.5753(3)	0.5753(3)
	z	0.3931(1)	0.3913(2)	0.3907(2)	0.3903(2)
	B_{eq}	0.58(2)	0.52(4)	0.62(4)	0.57(3)
O(1)	x	0.5719(4)	0.5645(8)	0.5650(6)	0.5633(6)
	y	0.7135(5)	0.7145(8)	0.7151(7)	0.7144(6)
	z	0.4711(3)	0.4699(4)	0.4694(4)	0.4683(4)
	B_{eq}	0.73(6)	0.61(9)	0.67(8)	0.67(8)
O(2)	x	0.8268(4)	0.8236(8)	0.8247(7)	0.8280(7)
	y	0.0070(4)	0.0081(8)	0.0101(7)	0.0099(6)
	z	0.5492(3)	0.5500(4)	0.5485(4)	0.5489(4)
	B_{eq}	0.55(5)	0.48(9)	0.74(8)	0.69(8)
O(3)	x	0.8350(4)	0.8338(9)	0.8311(6)	0.8297(7)
	y	0.7163(4)	0.7192(8)	0.7209(7)	0.7195(6)
	z	0.3362(3)	0.3358(4)	0.3341(4)	0.3335(4)
	B_{eq}	0.65(6)	0.64(9)	0.99(9)	0.95(9)
O(4)	x	0.5040(5)	0.4979(9)	0.4972(7)	0.4925(7)
	y	0.5041(5)	0.5071(9)	0.5062(7)	0.5066(6)
	z	0.2925(3)	0.2908(5)	0.2891(4)	0.2874(4)
	B_{eq}	0.82(6)	0.75(9)	0.79(9)	0.98(9)
O(5)	x	0.5375(5)	0.5336(9)	0.5329(7)	0.5338(7)
	y	0.9176(4)	0.9139(8)	0.9132(6)	0.9118(6)
	z	0.6563(3)	0.6583(5)	0.6581(4)	0.6582(4)
	B_{eq}	0.69(6)	0.75(9)	0.69(8)	0.81(8)
O(6)	x	0.8535(5)	0.8556(10)	0.8568(7)	0.8590(7)
	y	0.6736(5)	0.6715(8)	0.6698(7)	0.6707(7)
	z	0.6581(3)	0.6551(5)	0.6541(4)	0.6522(4)
	B_{eq}	0.86(6)	0.85(9)	0.94(9)	0.86(9)
O(7)	x	0.8019(5)	0.7992(8)	0.8007(7)	0.7990(7)
	y	0.3910(5)	0.3908(8)	0.3902(6)	0.3902(6)
	z	0.4634(3)	0.4618(4)	0.4612(4)	0.4610(4)
	B_{eq}	0.75(6)	0.51(9)	0.81(9)	0.83(8)

[a] X = Nd, Sm, Eu, Gd.

TABLE 3
Selected Bond Distances (Å) and Angles (°)

	$Nd_2Si_2O_7$	$Sm_2Si_2O_7$	$Eu_2Si_2O_7$	$Gd_2Si_2O_7$
X^a(1)–O(2)^{I}	2.428(3)	2.421(5)	2.390(4)	2.382(4)
X(1)–O(2)^{VI}	2.450(3)	2.426(5)	2.413(4)	2.377(4)
X(1)–O(3)^{II}	2.569(3)	2.553(5)	2.526(5)	2.510(5)
X(1)–O(3)^{V}	2.634(3)	2.606(5)	2.591(5)	2.594(4)
X(1)–O(4)^{II}	2.493(3)	2.477(5)	2.459(4)	2.456(4)
X(1)–O(5)	2.412(3)	2.374(6)	2.363(4)	2.363(4)
X(1)–O(6)^{IV}	2.638(3)	2.589(6)	2.575(4)	2.543(4)
X(1)–O(7)^{I}	2.331(3)	2.302(5)	2.285(4)	2.280(4)
Mean	2.494(2)	2.469(4)	2.450(3)	2.438(3)
X(2)–O(1)	2.640(3)	2.581(6)	2.575(4)	2.553(4)
X(2)–O(2)^{I}	2.500(3)	2.472(5)	2.461(4)	2.455(4)
X(2)–O(3)^{IV}	2.450(3)	2.408(6)	2.401(4)	2.391(4)
X(2)–O(4)	2.529(3)	2.497(5)	2.508(4)	2.492(4)
X(2)–O(4)^{III}	2.888(3)	2.864(6)	2.835(5)	2.810(5)
X(2)–O(5)^{II}	2.438(3)	2.392(5)	2.384(5)	2.372(4)
X(2)–O(6)^{I}	2.440(3)	2.395(5)	2.375(5)	2.373(4)
X(2)–O(6)^{II}	2.844(3)	2.901(6)	2.924(5)	2.956(4)
X(2)–O(7)^{I}	2.468(3)	2.445(5)	2.438(5)	2.425(4)
Mean	2.577(3)	2.551(4)	2.545(4)	2.536(3)
Si(1)–O(1)	1.652(4)	1.654(6)	1.643(5)	1.652(5)
Si(1)–O(2)	1.640(3)	1.623(5)	1.641(5)	1.648(5)
Si(1)–O(5)	1.602(3)	1.614(6)	1.610(5)	1.603(5)
Si(1)–O(6)	1.623(3)	1.615(6)	1.618(5)	1.607(5)
Mean	1.629(3)	1.627(5)	1.628(4)	1.627(4)
Si(2)–O(1)	1.648(4)	1.665(5)	1.652(5)	1.640(5)
Si(2)–O(3)	1.631(3)	1.632(6)	1.635(5)	1.629(5)
Si(2)–O(4)	1.624(4)	1.611(6)	1.608(5)	1.622(5)
Si(2)–O(7)	1.607(3)	1.597(6)	1.606(5)	1.600(5)
Mean	1.628(3)	1.626(5)	1.625(4)	1.623(4)
O(1)–Si(1)–O(2)	107.3(2)	107.9(3)	107.3(2)	107.5(2)
O(1)–Si(1)–O(5)	113.8(2)	112.7(3)	113.0(2)	113.0(2)
O(1)–Si(1)–O(6)	109.4(2)	108.9(3)	108.5(3)	108.2(2)
O(2)–Si(1)–O(5)	108.5(2)	109.0(3)	109.4(2)	109.9(2)
O(2)–Si(1)–O(6)	105.9(2)	105.7(3)	105.7(2)	104.3(2)
O(5)–Si(1)–O(6)	111.5(2)	112.2(3)	112.7(3)	113.3(3)
O(1)–Si(2)–O(3)	108.7(2)	108.5(3)	108.3(3)	108.6(2)
O(1)–Si(2)–O(4)	104.2(2)	102.8(3)	104.0(2)	103.5(2)
O(1)–Si(2)–O(7)	110.1(2)	110.2(3)	110.6(2)	110.6(2)
O(3)–Si(2)–O(4)	105.3(2)	106.0(3)	105.3(3)	105.0(3)
O(3)–Si(2)–O(7)	115.1(2)	115.2(3)	114.9(2)	114.9(2)
O(4)–Si(2)–O(7)	112.8(2)	113.3(3)	113.1(2)	113.4(2)
Si(1)–O(1)–Si(2)	124.4(2)	122.7(3)	123.4(3)	123.2(3)

Note. (I) $-x, -y, -z$. (II) $\frac{1}{2}+x, \frac{1}{2}-y, \frac{1}{2}+z$. (III) $\frac{1}{2}-x, \frac{1}{2}+y, \frac{1}{2}-z$. (IV) $x-1, y, z$. (V) $-x, -y+1, -z$. (VI) $x-1, y+1, z$.

[a] X = Nd, Sm, Eu, Gd.

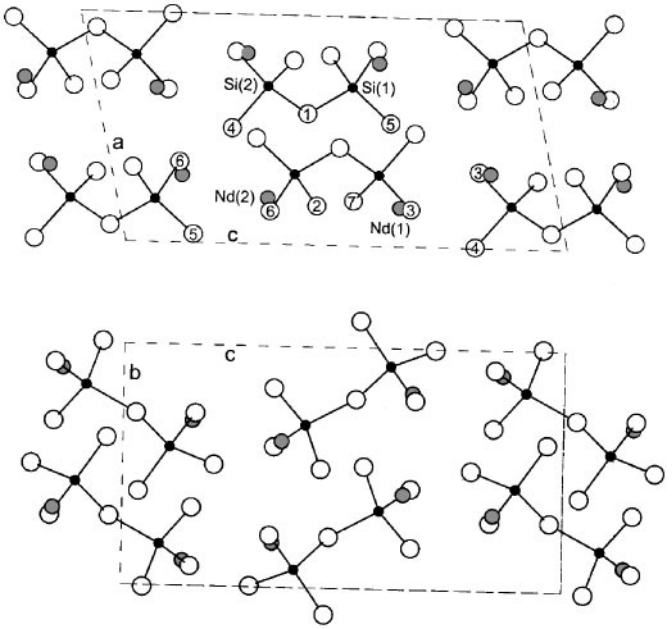

FIG. 1. Structure of high-pressure neodymium disilicate ($Nd_2Si_2O_7$) (type K): (a) (010) projection; (b) [100] projection.

an accelerating voltage of 20 kV, a beam current of 15 nA, a beam diameter of 2 μm, 20 s counts, and $NdPO_4$, $GdPO_4$, and albite ($NaAlSi_3O_8$) as standards; the measurements were reduced using the Love–Scott model (22). A crystal fragment of the Nd silicate gave a composition of Nd_2O_3 74.5(4) wt%, SiO_2 28.4(1) wt%, corresponding to a formula of $Nd_{1.87}Si_2O_7$, and a crystal fragment of the Gd silicate gave a composition of Gd_2O_3 74.6(3) wt%, SiO_2 26.1(5) wt%, corresponding to a formula of $Gd_{1.90}Si_2O_7$. The low contents of Nd and Gd were interpreted as an artifact of the analytical method used and particularly of the difficulty in calibrating EPMA for large amounts of heavy metals. The X-ray structure analyses (below) indicated that all four compounds presently investigated were indeed essentially stoichiometric.

Single-crystal measurements were made at room temperature and pressure with a Nonius Kappa CCD diffractometer and graphite-monochromatized Mo$K\alpha$ X-radiation (50 kV, 32 mA, $\lambda = 0.70926$ Å). Reflection data were processed with DENZO and SCALEPACK (University of Texas Southwestern Medical Centre at Dallas) and XDISPLAYF (University of Virginia Patent Foundation). Structure solution on high-pressure $Nd_2Si_2O_7$ and $Gd_2Si_2O_7$ was made with SHELXTL/PC (23) and all structure refinements were made with LINEX77 (State University of New York at Buffalo). Scattering factors for neutral atomic species and values of f' and f'' were taken, respectively, from Tables 2.2A and 2.3.1 of the International Tables for X-ray Crystallography (24). Relevant experimental details are given in Table 1, final parameters in Table 2, and selected bond distances and angles in Table 3.

RESULTS AND DISCUSSION

The disilicates of Nd, Sm, Eu, and Gd at 10 GPa have a new structure type (Table 1; Figs. 1–3), which we have

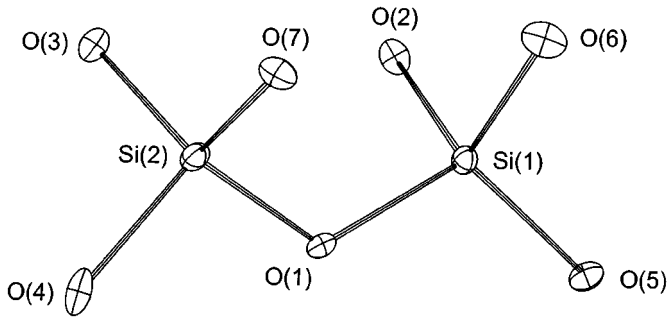

FIG. 2. Diorthosilicate group in high-pressure $Nd_2Si_2O_7$ (type K); thermal ellipsoids are scaled to enclose 50% probability; same view as in Fig. 1a.

designated "K". In omitting labels H and J from this series of rare earth disilicate structures we were misled by the use of "J-phase" for Yb N-woehlerite ($Yb_4Si_2O_7N_2$; e.g., Ref. (25)), but recognize that H and J will no doubt be used for new structure types at moderate pressure. All four crystals investigated were stoichiometric to within the resolution of the X-ray structure analyses. The maximum and minimum residual electron densities (Table 1) were located near rare earth cation positions, and they are typical of rare earth disilicate structures (e.g., Ref. (15)). The densities calculated from room pressure XRD measurements are 11–12% greater than those of the corresponding high-temperature, low-pressure polymorphs (type G for $Nd_2Si_2O_7$ and $Sm_2Si_2O_7$, type F for $Eu_2Si_2O_7$, and type E for $Gd_2Si_2O_7$) (Table 4), and there was no evidence of structural transformation, twinning, or strain in the X-ray diffraction patterns of the four crystals investigated. Hence, we feel that the type K structure is the structure type of these rare earth disilicates at the experimental pressure, and the four refined structures in Table 2 differ from those at 10 GPa only in respect to decompression of bond lengths and bond angles, the details of which are beyond the scope of the present study.

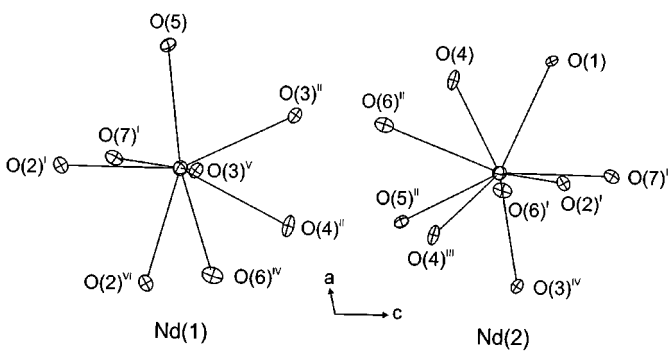

FIG. 3. Coordination environment of Nd in high-pressure $Nd_2Si_2O_7$ (type K); thermal ellipsoids are scaled to enclose 50% probability; same view as in Fig. 1a.

TABLE 4
Comparison of Structure Type, Unit-Cell Parameters, and Density

Type[a]	a (Å)	b (Å)	c (Å)	α (°)	β (°)	γ (°)	D_x (g/cm^3)
			$Nd_2Si_2O_7$				
A	6.7405	—	24.524	—	—	—	5.44
G	8.630	12.945	5.391	—	90.0	—	5.04
K	6.6658	6.7234	12.3975	—	102.147	—	5.584
			$Sm_2Si_2O_7$				
A	6.6933	—	24.384	—	—	—	5.70
F	8.513	12.867	5.374	91.34	92.06	90.43	5.26
G	8.564	12.855	5.383	—	90.0	—	5.23
K	6.6039	6.6849	12.3069	—	102.489	—	5.871
			$Eu_2Si_2O_7$				
B	6.716	6.762	12.321	94.36	90.02	91.75	5.62
A	6.6727	—	24.338	—	—	—	5.79
E	13.9142	5.0553	8.3486	—	—	—	5.33
F	8.517	12.848	5.385	91.65	92.24	90.44	5.33
K	6.5777	6.6652	12.2668	—	102.671	—	5.976
			$Gd_2Si_2O_7$				
B	6.624	6.679	12.132	94.10	89.79	91.60	5.99
E	13.8665	5.0532	8.3008	—	—	—	5.51
K	6.5558	6.6469	12.2394	—	102.844	—	6.166

[a] Structure type: A–G (1), all synthesized at 1 bar and listed in downward sequence of increasing temperature of stability; K from present study, synthesized at 10 GPa.

The new structure type is a diorthosilicate. It has some similarity to the type A structure (3, 5, 6), as is evident from comparison of unit-cell edge lengths (Table 4). However, such comparison can be ambiguous because the unit-cell parameters for the new structure type (K) are also similar to those of the type B structure, in which the silicate component is not diorthosilicate but a one-to-one combination of $[Si_3O_{10}]$ and isolated $[SiO_4]$ (7, 15). The REE^{3+} cations are located at either end of the diorthosilicate group (Fig. 1). The $X(1)$ cation is in irregular eightfold and the $X(2)$ cation in irregular ninefold coordination to 2.9 Å (Fig. 3; Table 3). The $X(2)$ cation is significantly under bonded (Table 5), and the mean $X(2)$–O distance is greater than the mean $X(1)$–O distance, suggesting that, in the decompressed structure, the nearest neighbor environment is too big for the REE^{3+} cation, and that the $X(2)$ polyhedron would be more compressible than $X(1)$. The mean REE^{3+}–O bond distances for $X(1)$ and $X(2)$ decrease progressively from $Nd_2Si_2O_7$ to $Gd_2Si_2O_7$ as expected, closely following the trend for variation of effective bond distance at given coordination number through the lanthanide series (e.g., Fig. 4). For the $X(1)$ position, the individual REE^{3+}–O bond distances decrease in proportion to decrease in the mean distance, but for $X(2)$ the decrease of individual REE^{3+}–O bond distances is not systematic. Whereas the change in mean bond distance from $Nd_2Si_2O_7$ to $Gd_2Si_2O_7$ is -0.041 Å, the change in

TABLE 5
Bond Valence Sums[a]

	$Nd_2Si_2O_7$	$Sm_2Si_2O_7$	$Eu_2Si_2O_7$	$Gd_2Si_2O_7$
X[b](1)	3.00	2.97	3.02	3.02
X(2)	2.82	2.86	2.83	2.82
Si(1)	3.94	3.98	3.96	3.97
Si(2)	3.96	3.99	3.99	4.02
O(1)	2.09	2.08	2.14	2.15
O(2)	2.15	2.17	2.14	2.14
O(3)	1.93	1.93	1.93	1.94
O(4)	1.82	1.84	1.84	1.80
O(5)	1.94	1.93	1.93	1.94
O(6)	1.81	1.83	1.82	1.85
O(7)	2.00	2.02	1.99	2.00

[a] Bond-valence parameters (26).
[b] X = Nd, Sm, Eu, Gd.

individual bond distances ranges from -0.087 Å for $X(2)$–O(1) to $+0.112$ Å for the long-distance $X(2)$–$O(6)^{II}$ (Table 3). On the other hand, the SiO_4 tetrahedra are fairly regular and their bond distances and bond angles do not vary in any systematic manner from $Nd_2Si_2O_7$ and $Gd_2Si_2O_7$. Also, note that both SiO_4 tetrahedra show the expected stretching of the bond to the bridging oxygen [O(1)],

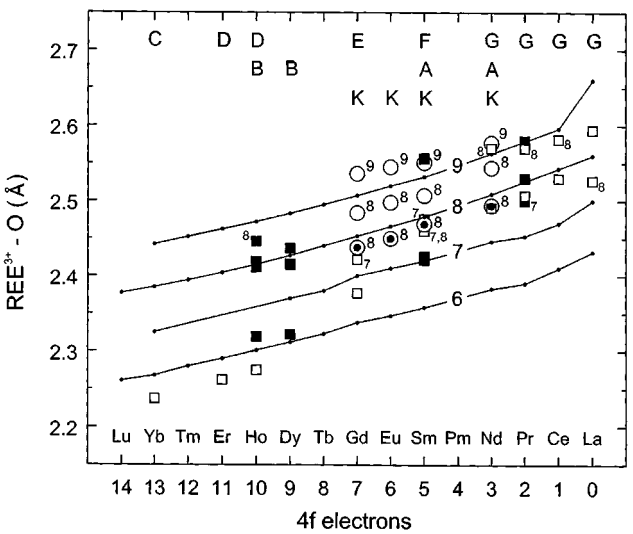

FIG. 4. Mean REE^{3+}–O bond distances of $X(1)$ and $X(2)$ polyhedra in type K disilicate structures of Nd, Sm, Eu, and Gd, and seven low-pressure disilicate structure types (A to G), relative to sum of effective cation-anion radii (16) for coordination numbers 6, 7, 8, and 9. Large open circles are eight- and ninefold coordination spheres of $X(2)$ and large centered circles are eightfold coordination spheres of $X(1)$ of type K phase, open small squares are structures of high-temperature phases (top row of structure type labels) and small full squares are structures of moderate-temperature phases; subscripts and superscripts are coordination numbers which, for low-pressure structure types, are indicated *only* for plots distant from their corresponding ideal trend (see Ref. (15)).

Fleet and Liu (15) compared the mean REE^{3+}–O distances of nonequivalent polyhedra in rare earth disilicate structures, recognizing that the outer limit of the nearest-neighbor coordination sphere of the large REE^{3+} cations is not well defined. They used an arbitrary limit of ≤ 2.8 Å to list REE^{3+}–O distances in the type B structure of $Dy_2Si_2O_7$. We have used a limit of 2.9 Å in this study, because the $X(2)$ environment includes two distances marginally longer than 2.8 Å. This arbitrary limit results in ninefold coordination for $X(2)$ (Figs. 3, 4), which may be rationalized on the basis that we have included all REE^{3+}–O distances inside of the next-nearest-neighbor coordination sphere comprised of Si(1) and Si(2). However, the 0.112 Å increase in the $X(2)$–$O(6)^{II}$ distance from $Nd_2Si_2O_7$ to $Gd_2Si_2O_7$ suggests that $O(6)^{II}$ is probably not part of the bonding sphere of the $X(2)$ cation. Therefore, the effective coordination of $X(2)$ may be eightfold rather than ninefold. The mean $X(2)$–O bond distances for eightfold coordination also plot parallel to the trend of the effective bond distances for this coordination (Fig. 4), but the mean distances for a coordination sphere limited to 2.8 Å (which results in sevenfold coordination for $X(2)$) do not, being close to the ideal distance for eightfold coordination in $Nd_2Si_2O_7$ and sevenfold coordination in $Gd_2Si_2O_7$. The average REE^{3+} cation coordination number in the type K structure appears to be eight, which is somewhat greater than those of the high-temperature, low-pressure disilicate structures of Nd, Sm, Eu, and Gd (which are between 7 and 8). Nevertheless, the REE^{3+}–O distances do not reveal evidence of anomalous compression in the high-pressure structure. The mean $X(1)$–O bond distances plot marginally below the ideal trend for eightfold coordination (Fig. 4), although they are not anomalous compared with mean distances for the low-pressure disilicate structures, and the mean $X(2)$–O bond distances plot above the ideal trends, for both eightfold and ninefold coordination spheres. Moving to the SiO_4 tetrahedra, the polyhedral volumes (which are 2.213, 2.203, 2.208, and 2.201 Å^3 for Si(1), and 2.199, 2.191, 2.189, and 2.178 Å^3 for Si(2) in $Nd_2Si_2O_7$, $Sm_2Si_2O_7$, $Eu_2Si_2O_7$, and $Gd_2Si_2O_7$, respectively) and distortion parameters are also not anomalous, compared with low-pressure rare earth silicate structures in general. In summary, the average REE^{3+} cation coordination number in the type K structure is marginally greater than in comparable low-pressure structures, but the other geometrical characteristics of the REE^{3+} cation and Si polyhedra, as measured at 1 bar, do not reveal evidence for the high-pressure stability of this phase.

In contrast, the dihedral angle in the diorthosilicate group of the type K structure is significantly reduced relative to comparable low-pressure structures (Fig. 5). In the low-pressure structures, the dihedral angle varies markedly with size of REE^{3+} cation, being about 130–135° in disilicates of

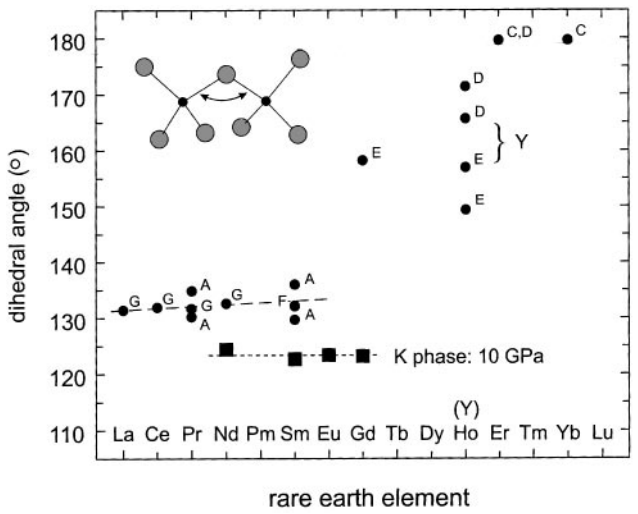

FIG. 5. Variation of bridging oxygen (Si–O–Si) bond angle in diorthosilicate group of type K disilicate structures of Nd, Sm, Eu, and Gd, compared with data for low-pressure *REE* disilicate structures (type A to G): note that the distribution for the low-pressure structures hinges at a dihedral bond angle of ~140°, which is considered to be the strain-free value (27), and that in the high-pressure structures (type K) densification is accomplished by further bending of the dihedral bond angle.

the light rare earths and increasing to 180° in the type C phase of $Er_2Si_2O_7$ and $Yb_2Si_2O_7$. The energy of an isolated or hydrogen-saturated polymerized silicate group is well known to vary with Si–O–Si angle at given Si–O bond distance (e.g., Ref. (28)). For the $H_6Si_2O_7$ molecule, the minimum energy occurs at a dihedral angle of about 140° (for Si–O bond distances near 1.62 Å). The mean value of the bridging oxygen (Si–O–Si) bond angle for all silicate structures is also near 140°, and Liebau (27) suggested that this was the strain-free value for the Si–O–Si bond angle in silicates in general. It is, perhaps, not coincidental that the change in slope of the dihedral bond angle distribution for the low-pressure rare earth disilicates (near Gd) also occurs at about 140°. Evidently the heavy rare earth cations (Lu–Er) are too small to interconnect diorthosilicate groups in simple packing models without straightening the dihedral angle. Conversely, the light rare earth cations (La–Sm) are too large and cause the dihedral angle to be bent to accommodate their larger cation polyhedra.

Loriers *et al.* (29) used similar but qualitative reasoning in their crystal-chemical discussion of the pressure stability of the disilicates of Tm, Yb, and Lu (30) at 1 bar to 7.0 GPa. The type B phase was stable at the highest pressure investigated, and a new structure type (X) replaced type C at moderate temperature and pressure. It was suggested that the phase transition sequence C → X → B with increase in pressure was accompanied by closure of the Si–O–Si bond angle, as in this study, and increase in the coordination of the REE^{3+} cation from 6 to 7 and then 8. The type X structure was not determined but was believed to be the silicate analogue of $Er_2Ge_2O_7$ (31), which has a dihedral (Ge–O–Ge) bond angle of 136°.

We conclude that the type K structure is a high-pressure modification because the diorthosilicate group is compressed along its long axis by closure of the dihedral angle and the average coordination number of the REE^{3+} cations is increased to 8. Decrease in the dihedral angle is accomplished essentially by rigid body rotation of the two SiO_4 tetrahedra, and this allows both of the REE^{3+} cations to be accommodated in eightfold coordinated polyhedra. Interestingly, the bulk composition $La_2O_3.2SiO_2$ does not form a disilicate at 10 GPa (and 1600–1700°C) (work in progress). This is no doubt because the La^{3+} cation is too large to be accommodated by closure of the dihedral angle.

ACKNOWLEDGMENTS

We thank three unnamed reviewers for helpful comments, Michael Jennings for assistance with collection of X-ray reflection data, Yves Thibault for assistance in EPMA, and the Natural Sciences and Engineering Research Council of Canada for financial support.

REFERENCES

1. J. Felsche, *J. Less-Common Met.* **21,** 1 (1970).
2. J. Felsche, *Naturwiss.* **57,** 452 (1970).
3. J. Felsche, *Naturwiss.* **57,** 669 (1970).
4. Yu. I. Smolin and Yu. F. Shepelev, *Acta Crystallogr. Sect. B* **26,** 484 (1970).
5. Yu. I. Smolin, Yu. F. Shepelev, and I. K. Butikova, *Soviet Phys. Crystallogr.* **15,** 214 (1970).
6. J. Felsche, *Z. Kristallogr.* **133,** 364 (1971).
7. J. Felsche, *Naturwiss.* **59,** 35 (1972).
8. J. Felsche, *in* "Structure and Bonding" (J. D. Dunitz, Ed.), p. 99, Vol. 13. Springer-Verlag, Berlin, 1973.
9. O. Greis, H. G. Bossemeyer, P. Greil, B. Breidenstein, and A. Haase, *Mater. Sci. For.* **79–82,** 803 (1991).
10. H. W. Dias, F. P. Glasser, R. P. Gunwardane, and R. A. Howie, *Z. Kristallogr.* **191,** 117 (1990).
11. A. N. Christensen, *Z. Kristallogr.* **209,** 7 (1994).
12. A. N. Christensen and R. G. Hazell, *Acta Chem. Scand.* **48,** 1012 (1994).
13. A. N. Christensen, R. G. Hazell, and A. W. Hewat, *Acta Chem. Scand.* **51,** 37 (1997).
14. A. N. Christensen, A. F. Jensen, B. K. Themsen, R. G. Hazell, M. Hanfland, and E. Dooryhee, *Acta Chem. Scand.* **51,** 1178 (1997).
15. M. E. Fleet and Xiaoyang Liu, *Acta Crystallogr. Sect. B* **56,** 940 (2000).
16. R. D. Shannon, *Acta Crystallogr. Sect. A* **32,** 751 (1976).
17. H. D. Megaw, "Crystal Structures: A Working Approach." Saunders, Philadelphia, 1973.
18. R. M. Hazen and L. W. Finger, "Comparative Crystal Chemistry." Wiley, New York, 1982.
19. M. T. Dove, V. Heine, and K. D. Hammonds, *Miner. Mag.* **59,** 629 (1995).
20. M. T. Dove, *Am. Miner.* **82,** 213 (1997).
21. M. J. Walter, Y. Thibault, K. Wei, and R. W. Luth, *Can. J. Phys.* **73,** 273 (1995).

22. D. A. Sewell, G. Love, and V. D. Scott, *J. Phys. D* **18,** 1233 (1985).
23. Siemens, "SHELXTL PC," Version 4.1. Siemens Analytical X-ray Instruments, Inc., Madison, WI, 1993.
24. J. A. Ibers and W. C. Hamilton (Eds.), "International Tables for X-ray Crystallography," Vol. IV. Kynoch Press, Birmingham, UK, 1974.
25. V. A. Izhevskii, *Powder Metall. Metal Cer.* **37,** 67 (1998).
26. N. E. Brese and M. O'Keeffe, *Acta Crystallogr. Sect. B* **47,** 192 (1991).
27. F. Liebau, "Structural Chemistry of Silicates." Springer-Verlag, Berlin, 1985.
28. G. V. Gibbs, J. W. Downs, and M. B. Boisen, Jr., *in* "Reviews in Mineralogy" (P. J. Heaney, C. T. Prewitt, and G. V. Gibbs, Eds.), Vol. 29, p. 331. Mineralogical Society of America, Washington, 1994.
29. J. Loriers, G. Bocquillon, C. Chateau, and D. Colaïtis, *Mater. Res. Bull.* **12,** 403 (1977).
30. G. Bocquillon, C. Chateau, C. Loriers, and J. Loriers, *J. Solid State Chem.* **20,** 135 (1977).
31. Yu. I. Smolin, *Soviet Phys. Crystallogr.* **15,** 36 (1970).